

This is an Open Access document downloaded from ORCA, Cardiff University's institutional repository: <https://orca.cardiff.ac.uk/id/eprint/128791/>

This is the author's version of a work that was submitted to / accepted for publication.

Citation for final published version:

Chong, Cheng Tung, Chiong, Meng-Choung, Teyo, Zhe Yong, Ng, Jo-Han, Chong, William Woei Fong, Tran, Manh-Vu, Lam, Su Shiung and Valera Medina, Agustin 2020. Pool fire burning characteristics of biodiesel. *Fire Technology* 56 , pp. 1703-1724. 10.1007/s10694-020-00949-3

Publishers page: <http://dx.doi.org/10.1007/s10694-020-00949-3>

Please note:

Changes made as a result of publishing processes such as copy-editing, formatting and page numbers may not be reflected in this version. For the definitive version of this publication, please refer to the published source. You are advised to consult the publisher's version if you wish to cite this paper.

This version is being made available in accordance with publisher policies. See <http://orca.cf.ac.uk/policies.html> for usage policies. Copyright and moral rights for publications made available in ORCA are retained by the copyright holders.



# Pool Fire Burning Characteristics of Biodiesels

## Abstract

The characteristics of pool fire burning of methyl esters/biodiesels of palm, soybean, coconut and their blends with diesel were compared against baseline diesel. Pool fires were established and investigated using four different crucible sizes, ranging between 40 and 70 mm in diameter to obtain the mass burning rate, flame height and emissions of NO, CO, and SO<sub>2</sub> under diffusional flame mode at unconfined atmospheric conditions. The mass burning rate increased with increasing crucible size for all tested fuels, with biodiesel showing higher mass burning rates when compared with diesel. Modified empirical correlations for estimating fuel mass burning rate and flame height showed good agreement with experimental data. Emission-wise, biodiesels generally exhibited higher specific NO emission level than baseline diesel. Blending biodiesel with diesel resulted in an increase of NO level. CO emissions showed a reverse trend, where diesel showed higher emission values than all biodiesels. Burning of neat palm and coconut biodiesels showed non-existent SO<sub>2</sub> emission. The experiment showed that the oxygen content in biodiesel assists in pool fire combustion, as evident by the higher mass burning rate as compared to diesel. Soybean biodiesel with higher density exhibited higher mass burning rate as compared to palm and coconut biodiesels. Biodiesel with high level of unsaturation produced lower NO but higher CO emissions.

*Keywords: Pool fire; Biodiesel; Emissions; Safety; Mass burn rate; Flame height*

## 1.0 Introduction

Biodiesel is an oxygenated, renewable and biodegradable alternative fuel that has shown to produce considerably lower soot, unburned hydrocarbons (UHC) and particulate matter (PM) than diesel [1, 2]. In addition, biodiesels also possess very similar cetane number (CN), calorific value and viscosity to diesel, making them a favoured alternative fuel to fulfil the energy demand in many countries [2]. Recent outlooks have projected that energy demand for biodiesels is expected to grow by a factor of approximately 7 by year 2035 [3]. With growing popularity in the use of biodiesel, safety concerns on biodiesel also increase. Biodiesel spills could happen just like fossil fuel during handling or transportation, resulting in hazardous pool fires that may cause serious catastrophes. It is therefore imperative to understand the pool fire characteristics of biodiesel.

There have been numerous studies on petroleum fuel pool fire characteristics. The effect of different pan diameters on mass burning rate were studied [4, 5]. These studies showed that mass burning rate of the fuels escalate as the pan diameter increased, owing to the greater surface area available for burning. Meanwhile, fuel density is another controlling parameter that affects the mass burning rate [6]. Higher density fuels were found to render higher amounts of mass whilst burning at a fixed area, elevating mass burning rate inherently. To simulate a more practical case, a longitudinal wind flow was added to the study of n-heptane pool fires and its effect on mass burning rate was investigated [7, 8]. It was found that increasing the longitudinal air velocity increases the fuel mass burning rate for a given pool size. However, this was only valid when heat release rate prevails the cooling effect from accelerated air flows. In another investigation on longitudinal air flow effects, it was found that for a given pool size, the mass burning rate for a small square pool (7.5 cm and 10 cm) increases almost monotonically with increasing air speed [9]. However, for a 30 cm square pool the mass burning rate was found independent of the air flow velocity [9]. Conversely, Hu et al. [10]

reported that for square pools smaller than 30 cm, fuel mass burning rates vary non-monotonically with increasing air speed. For air velocities from 1.1 m/s to 3.1 m/s, fuel mass burning rate exhibits linear decreasing trends from square pools between 5 and 15 cm. Conversely, fuel mass burning rates show linear increasing trends as the square pool increases from 15 to 25 cm [10, 11]. Fuel mass burning rates for all crucibles were found higher than that of quiescent air [10, 11]. Therefore, air flows introduce greater amount of oxygen into the flame, elevating the flame temperature and heat transfer efficiency from the flame to the fuel surface. In addition, deflection of the flame also increases at higher air flows, thus heating up the pool rim and promoting heat transfer to the fuel [8, 12, 13].

Estimating the flame height of a pool fire is of essential importance as it determines how the flame would interact with its surrounding. Thomas et al. [14] first derived basic parameters that determine the flame height. These parameters include pool diameter, mass burning rate, fuel density, gravity and the expansion coefficient of air. Heskestad [15] examined data from several published works and found that the normalised flame height ( $L/D$ ) is proportional to the fuel burning rate parameter ( $\dot{Q}^2/D^5$ ), where  $L$  is flame height,  $D$  is pool diameter and  $\dot{Q}$  is heat releases rate. The effect of gravity on flame height was examined by Ito et al. [16, 17]. The effect of low gravity level (non-dimensional gravity level,  $G < 1$ ) was considered using crucible diameters ranging from 20 to 40 mm. Flame height variations of acetone, n-heptane, kerosene against gravity level 0.55-0.70 were studied. It was reported that the flame height exhibits linear correlation to gravity levels with a gradient of 1/4. The effect of the crucible aspect ratio,  $n$  (ratio between long side and short side length of the crucible), on flame height was examined by Tu et al. [18]. It was demonstrated that using ethanol and n-heptane pool fires that the flame height exhibited decreasing trends as the crucible aspect ratio increased. The flame height for n-heptane and ethanol decreased by a factor of roughly 1.25 and 2.6, respectively, as  $n$  increased from 1 to 8. Tang et al. [19] reported in year 2015 that the

flame height for acetone pool fires was marginally higher under atmospheric conditions (1 bar) than that of sub-atmospheric (0.64 bar) cases. At cross flow air velocities of 0.5 m/s and crucible aspect ratios of 8 the flame height under atmospheric conditions was approximately 0.02 m higher than that of sub-atmospheric condition. This is mainly due to the lower air density and entrainment at sub-atmospheric condition.

Smoke is the combination of soot and toxic gaseous products from burning materials [20]. These gaseous products comprised of nitric oxide (NO), carbon monoxide (CO), and sulphur dioxide (SO<sub>2</sub>) present great threats to individuals involved in fires. It was reported that more than 50% of all fatalities can be attributed to the inhalation of smoke and toxic gas in the UK and US cases [20]. It is possible to determine available safe egress time, i.e., the time between fire detection and the onset of conditions which are hazardous to continued human occupancy, based on the rate of fire and emissions growth [20]. Considering these aspects, emissions from the various pool fires have been quantified by several works. Koseki and Mulholland [4] demonstrated using crude oil pool fires whose concentration of CO in the smoke exhibits exponential growth as crucible diameter increased from 0.6 to 3 m. Smith and Cox [21] reported that peak CO concentration takes place at farther fuel-rich concentrations than the stoichiometric mixture fraction. Chen et al. [22] found that CO concentration increases linearly with increasing radiant heat flux for diesel, kerosene and lubricating oil pool fires. Carbon monoxide concentration for diesel was found to be higher than kerosene by a factor of 1.46 at 10 kW/m<sup>2</sup> radiant heat flux. Tran et al. [23] showed that for pool diameters of 57 mm, CO emissions from diesel are higher than SME by a factor of approximately 4.5. Nitrogen oxide emissions for SME were only marginally higher when compared with those of diesel.

The burning characteristics of biodiesel under a pool fire configuration has received comparatively lesser attention than diesel. Biodiesel can be produced from a variety of feedstocks characterised by a wide range of fatty acid compositions. Thus, it is of no surprise

that the properties of biodiesels exhibit different physical, chemical and burning characteristics. For example, the level of unsaturation degree in biodiesel was shown to be a major reason for the change in nitrogen oxide ( $\text{NO}_x$ ) emissions [24] and soot [25]. Tran et al. [23] showed that diesel fuel blended with higher fractions of biofuel resulted in lower level of mass burning rates, marginally decreasing flame height in a diffusion pool flame configuration. In a biodiesel pool fire study, the mass burning rate of biodiesel was shown to differ with fuel thickness and pool size [26], but the study on the influence of degree of unsaturation was not investigated.

In the present work, three biodiesels of varied unsaturation degree, notably palm (PME), coconut (CME) and soybean methyl ester/biodiesels (SME) are used to establish pool fires to investigate their burning characteristics. The effects of physical and chemical properties on flame height, appearance, mass burning rate and emissions are compared with baseline diesel. The data obtained can serve as validation targets for biodiesel pool flame modelling, as well as reference for storage, handling and transporting.

## **2.0 Experimental**

### **2.1 Fuel Preparation**

Biodiesels of soybean, coconut and palm were produced in-house using cooking oil via the transesterification process. The cooking oil was initially heated up to 60 °C before mixing with blends of methanol and potassium hydroxide (KOH) at the ratio of 113.7:50:1 by mass. A magnetic stirrer was used to stir the mixture at 60 °C for 3 hours. The blended mixture was collected after 3 hours and was left overnight to allow separation of biodiesel and glycerol. The formed biodiesel located on the top layer was poured into a clean beaker and heated up to 120 °C for 4 hours to vaporise the water and methanol. The produced biodiesels were characterised using a gas chromatography (GC, Agilent 7620A) based on standard EN 14103. The GC result shows that 98% biodiesel yield was achieved. The standard diesel used as baseline was purchased from a local petrol station.

### **2.2 Fuel Properties**

Biodiesel consists of a mixture of fatty acid methyl esters. Biodiesels produced from palm, soy and coconut are also known as palm methyl esters (PME), soybean methyl esters (SME) and coconut methyl esters (CME), respectively. The approximated fatty acid compositions for PME, SME and CME are shown in Table 1. Fatty acid analysis shows that CME is composed of shorter chain fatty acids as compared to SME and PME. SME consists of a high level of fatty acids with double bonds, while CME contains the least unsaturated fatty acids. This fact results in the low unsaturation degree of CME compared to SME, while the PME's saturation level is in-between. The fuel physical and chemical properties of all biodiesels and diesel are shown in Table 2. Biodiesel is notably less volatile and shows higher

viscosity than diesel. The lower volatility of biodiesel results in higher flash point as compared to diesel. Due to the presence of oxygen in biodiesel, the caloric value for biodiesel is roughly 12.3-17.3% lower than diesel on mass basis. The molecular weight for biodiesel is generally higher than diesel, hence the density is higher for the former.

Table 1 Percentage of fatty acids composition in PME, SME and CME.

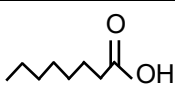
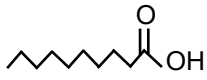
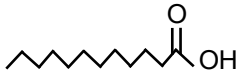

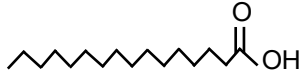

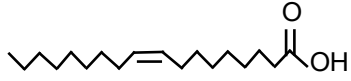
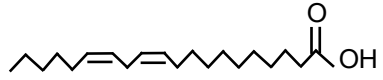
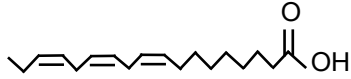
Fatty Acid	No of Carbon: double bond	Structure	Composition (% wt)		
			PME	SME	CME
Caprylic	(C8:0)		0.8	-	6.8
Capric	(C10:0)		-	-	5.4
Lauric	(C12:0)		-	0.1	47.7
Myristic	(C14:0)		1.1	0.1	18.5
Palmitic	(C16:0)		42.5	11.6	9.1
Stearic	(C18:0)		4.2	3.9	2.7
Oleic	(C18:1)		41.3	23.7	6.8
Linoleic	(C18:2)		9.5	53.8	2.1
Linolenic	(C18:3)		-	5.9	0.1
Others			0.6	0.9	0.8



Table 2 Physical properties for diesel, PME, SME and CME.

Properties	Unit	Diesel	PME	SME	CME
C <sup>†</sup>	[% wt]	87.4	76.0	77.2	73.9
H <sup>†</sup>	[% wt]	12.6	12.2	11.8	12.1
O <sup>†</sup>	[% wt]	0.0	11.8	11.0	14.0
Lower Heating Value <sup>†</sup>	[MJ/kg]	42.6	37.4	37.0	35.2
Density <sup>†</sup>	[kg/m <sup>3</sup> ]	843.3	867.7	882.0	874.0
CN <sup>††</sup>	[-]	50.0	62.0	47.0	59.3
Flash Point <sup>††</sup>	[°C]	65.0	163.0	159.0	113.0
Kinematic Viscosity <sup>††</sup> (40°C)	[mm <sup>2</sup> /s]	2.7	4.6	4.3	2.8
Molecular Weight <sup>*</sup>	[g/mol]	226.0	270.1	292.2	229.1

<sup>†</sup> Measured

<sup>††</sup> Taken from [27, 28]

<sup>\*</sup> Calculated

### 2.3 Experimental and measurement techniques

Four circular stainless-steel crucibles with inner diameters of 40 to 70 mm were used to investigate the pool fire behaviour of the various tested biodiesels. The depth for all crucibles was 26 mm. To establish a pool fire, the crucible was filled with liquid fuel, then it was placed on a hot plate and heated to the temperature of the fuel's flash point. An infrared thermometer (BENETECH GM320) was used to monitor the fuel temperature. The pool fire was then ignited and stabilised with a flame torch. Fig. 1 shows the schematic of the experimental setup.

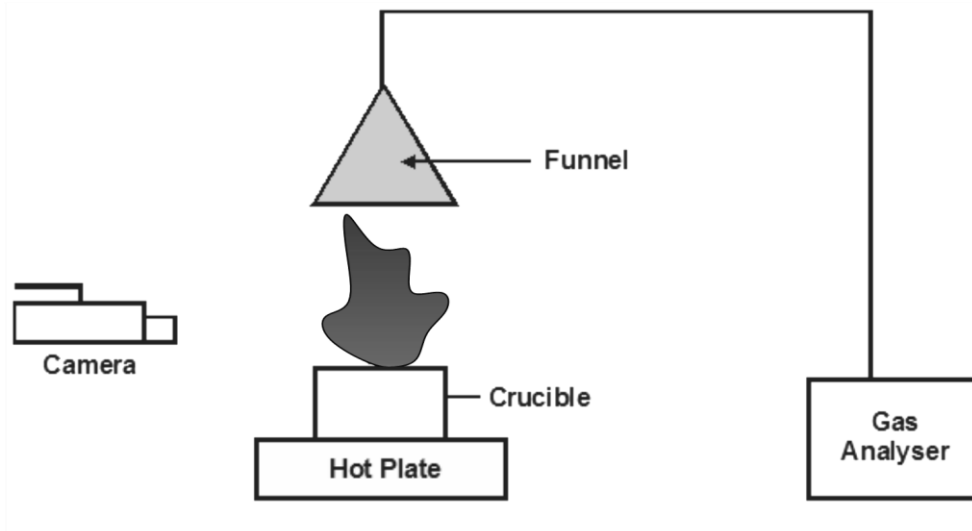


Fig. 1 Schematic diagram of experimental setup.

The mass burning rate (MBR) of liquid fuel was calculated based on the equation  $MBR = \frac{m_i - m_f}{\Delta t}$ , where  $m_i$  is the initial mass of the fuel,  $m_f$  is the final mass of fuel and  $\Delta t$  is the time interval. The mass of the fuel was measured by using a weighing scale, while the mass burning rates were determined after 10 minutes of burning the pool. The global flame appearance was recorded using a SONY NEX-5 digital camera at 30 fps frame rate and 1920 x 1080 resolution. The mean flame height was determined based on the 0.5 intermittency criteria due to the pulsating nature of the fire plume [29, 30]. The intermittency refers to the fraction of time at which part of the flame is higher than a specific vertical elevation,  $z$ , from the fire source [29, 30]. The post-combustion emission products of nitric oxide (NO), carbon monoxide (CO), and sulphur dioxide (SO<sub>2</sub>) were measured using a gas analyser (ECOM J2KN Pro). Calibration gases were used to calibrate the gas analyser prior to measurements. The sampling tube has an inlet diameter of 5 mm. The probe continuously samples for 2 minutes to allow readings to reach steady state condition. The emissions measured include NO, CO and

SO<sub>2</sub>. The range of measurements, resolution, uncertainty and propagated errors of the gas analyser are summarised in Table 3.

Table 3 Gas analyser specification.

<b>Sensor</b>	<b>Range</b>	<b>Resolution</b>	<b>Uncertainty</b>	<b>Propagated Error</b>
NO	0-5000 ppm	1 ppm	± 5 ppm	30.3 %
CO	0-4000 ppm	1 ppm	± 5 ppm	0.82 %
SO <sub>2</sub>	0-5000 ppm	1 ppm	± 5 ppm	12.34 %

### 3.0 Results and Discussions

#### 3.1 Mass Burning Rate

Mass burning rate (MBR) is an important parameter for quantifying the size of the pool fire and determining the radiative heat flux received by the nearby combustible items [20]. The effect of increasing biodiesel percentage in diesel on fuel mass burning rate is shown in Fig. 2. Overall, the neat biodiesels (B100) show overall higher burning rates than B20 (20/80 biodiesel/diesel blend) for all crucibles shown. For the 40 mm crucible, MBR for CME, SME and PME blends increase by a factor of approximately 1.1-1.4 from B20 to B100. Among the blends, there is no clear distinction between the mass burning rates. CME blends show slightly higher burning rates than PME and SME blends for 50 and 70 mm crucibles but the difference is not evident for 40 mm crucible. PME blends show lower mass burning rates for the 50 mm crucible, but much closer to CME and SME counterparts when burning with other crucibles. It is noted that the measured MBR values such as those exhibited by PME B60 in Fig. 2b does not fall within the expected linear trends. This is believed to be caused by random errors such as uneven vaporisation of the fuel on the pool surface, leading to pulsed uneven burning rates based on convection of the vapour that caused the flame to flicker. Another possible reason is the effect of ambient draft that affects the burning rate. These effects were not quantifiable in the current setup, although they may have contributed to these deviations.

Comparison of the MBR between neat biodiesels and diesel at different crucible sizes is shown in Fig. 3. The burning rate for all fuels increases with the increase of crucible size, owing to the larger surface area available for burning [4]. This renders higher heat transfer rate from the flame to the liquid fuel pool surface, promoting fuel vaporisation on the pool surface which leads to higher burning rate. It was previously identified that conduction is the main heat transfer mechanism for crucibles with an equivalent diameter ( $D_{eq}$ ) much smaller than 1 m, while heat transfer via convection and radiation prevails as  $D_{eq}$  increases [31].

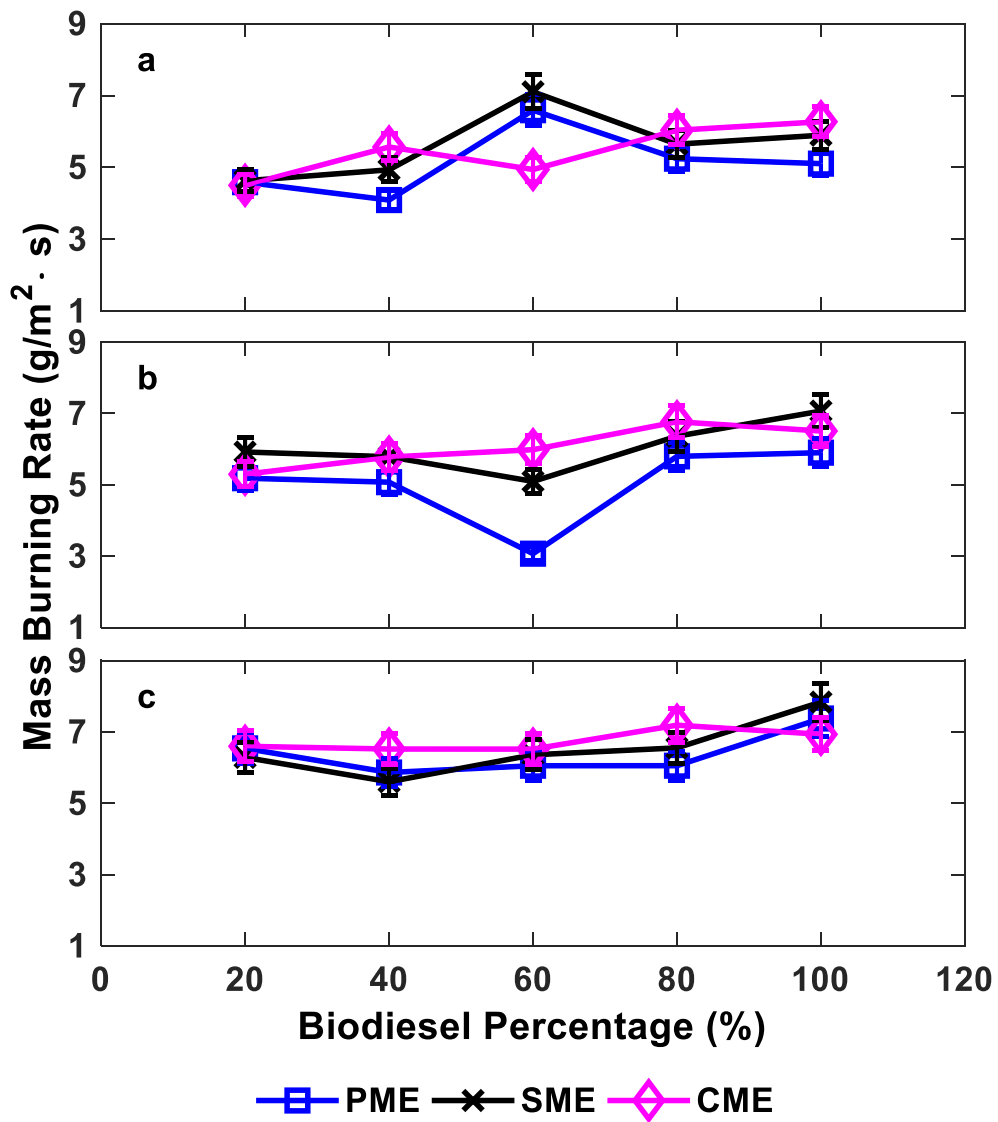


Fig. 2 Mass burning rate of different blend percentage of PME, SME and CME in diesel for (a) 40, (b) 50 and (c) 70 mm crucibles.

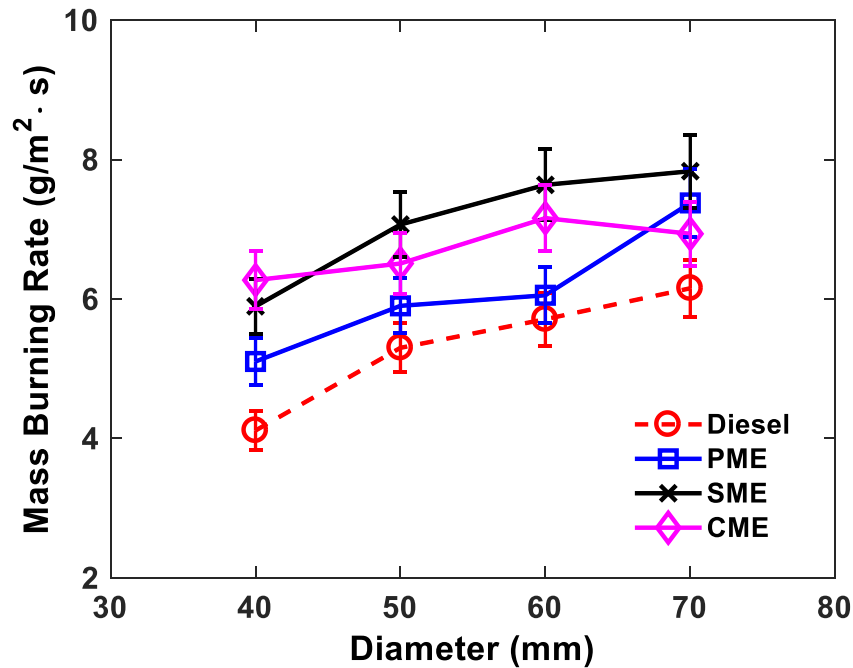


Fig. 3 Comparison of mass burning rate between PME, SME, CME and baseline diesel for different crucible sizes.

The MBR for diesel is consistently lower than all biodiesels for all crucible sizes, partly due to the higher density of biodiesels that renders more fuel mass to be consumed for a given surface area as compared to diesel. Furthermore, combustion of diesel resulted in sootier flames than those from biodiesels [32]. Sootier diesel flames may incur higher radiative heat loss and cause the flame to burn at lower temperature [33], hence the amount of heat transferred back to the pool surface via conduction is reduced, resulting in lower MBR as the fuel decomposition rate is lower. For biodiesel, the presence of fuel-bond oxygen results in more complete combustion, thus the flame temperature is expected to be higher than diesel [33]. As a result, more heat is conducted back to the pool surface, causing higher MBR when compared with that of diesel.

Among the tested biodiesels there is no distinct trend in the burning rates. The highly unsaturated SME tends to show slightly higher burning rates (except for a crucible diameter of 40 mm), while PME with a medium saturation level shows the lowest burning rate. CME,

which contains the highest oxygen to carbon (O/C) ratio, is expected to have lower radiative heat loss due to higher soot oxidation rates [33]. SME with higher unsaturation degree is expected to be sootier and may cause higher radiative heat losses [25, 33]. This fact should lead to lower heat conduction for SME and subsequently lower its MBR. However, the trend indicates the opposite, thus neither the heat transfer nor the chemistry are the dominant effects that control the biodiesel MBR. The higher density of SME could be the primary factor that promotes fuel burning rates, causing a slightly higher burning rate than CME and PME.

Fuel MBR is of importance in determining the amount of radiative heat flux delivered to the adjacent pool surface [20]. The MBR of fuel ( $\dot{m}$ ) is thus estimated based on the empirical equation (Eq. 1) [34]

$$\dot{m} = \dot{m}_{\infty} [1 - e^{(-kD_{eq})}] \quad (1)$$

where  $\dot{m}_{\infty}$  and  $k$  are maximum MBR and rate of growth, respectively. The present study shows that  $\dot{m}_{\infty}$  and  $k$  in Eq. 1 are correlated to the fuel density ( $\rho_f$ ) via empirical correlations as shown in Fig. 4, where both  $\dot{m}_{\infty}$  and  $k$  are linear functions of  $\rho_f$ .

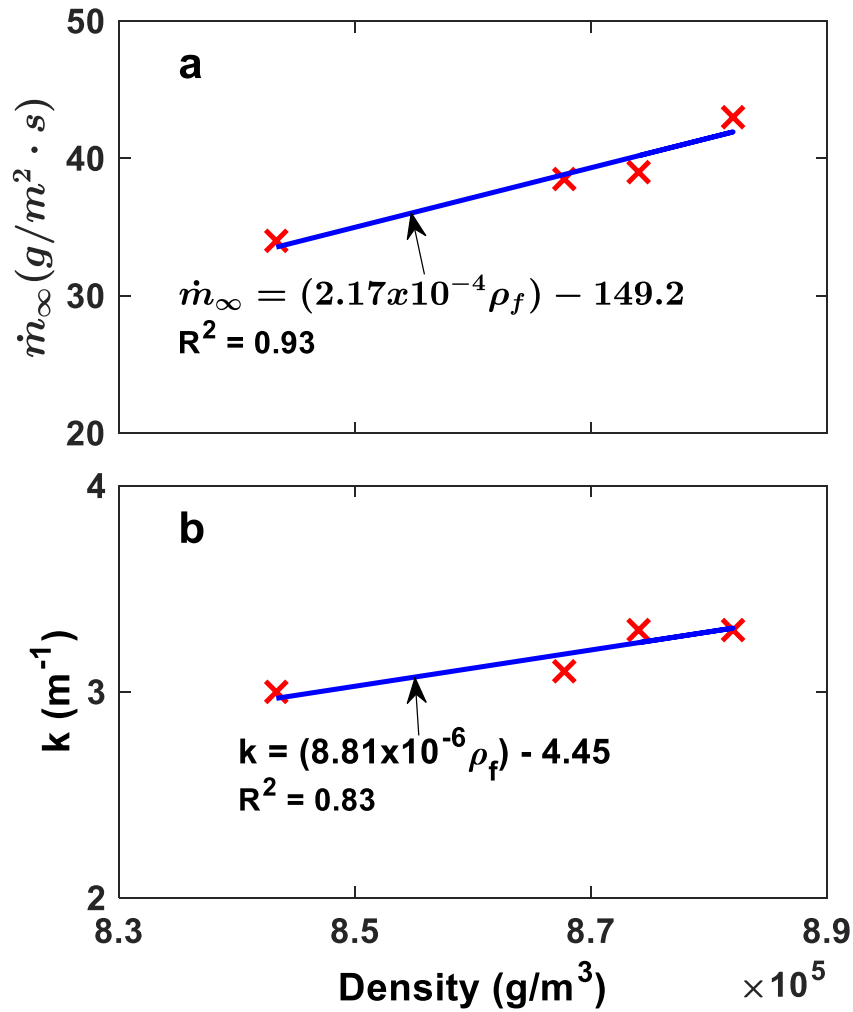


Fig. 4 Correlation of (a)  $\dot{m}_\infty$  and (b)  $k$  as a function of fuel density.

Eq. 1 is subsequently revised using the empirical correlations delineated in Fig. 4. The revised correlation is supported by the fact that fuel density is known to be an important controlling parameter that affects mass burning rate [6]. Figure 5 shows how the modified Eq. 1 predicts the experimental MBR reasonably well. The soy biodiesel MBR produced by Tran et al. [23] is included in Fig. 5c for validation purposes. The empirical models shown in Fig. 4 are sufficiently reliable to estimate the  $\dot{m}_\infty$  and  $k$  for diesel and biodiesels of different feedstock for crucible inner diameters of  $40 \text{ mm} < D_{\text{eq}} < 70 \text{ mm}$ , given that  $\rho_f$  is known.



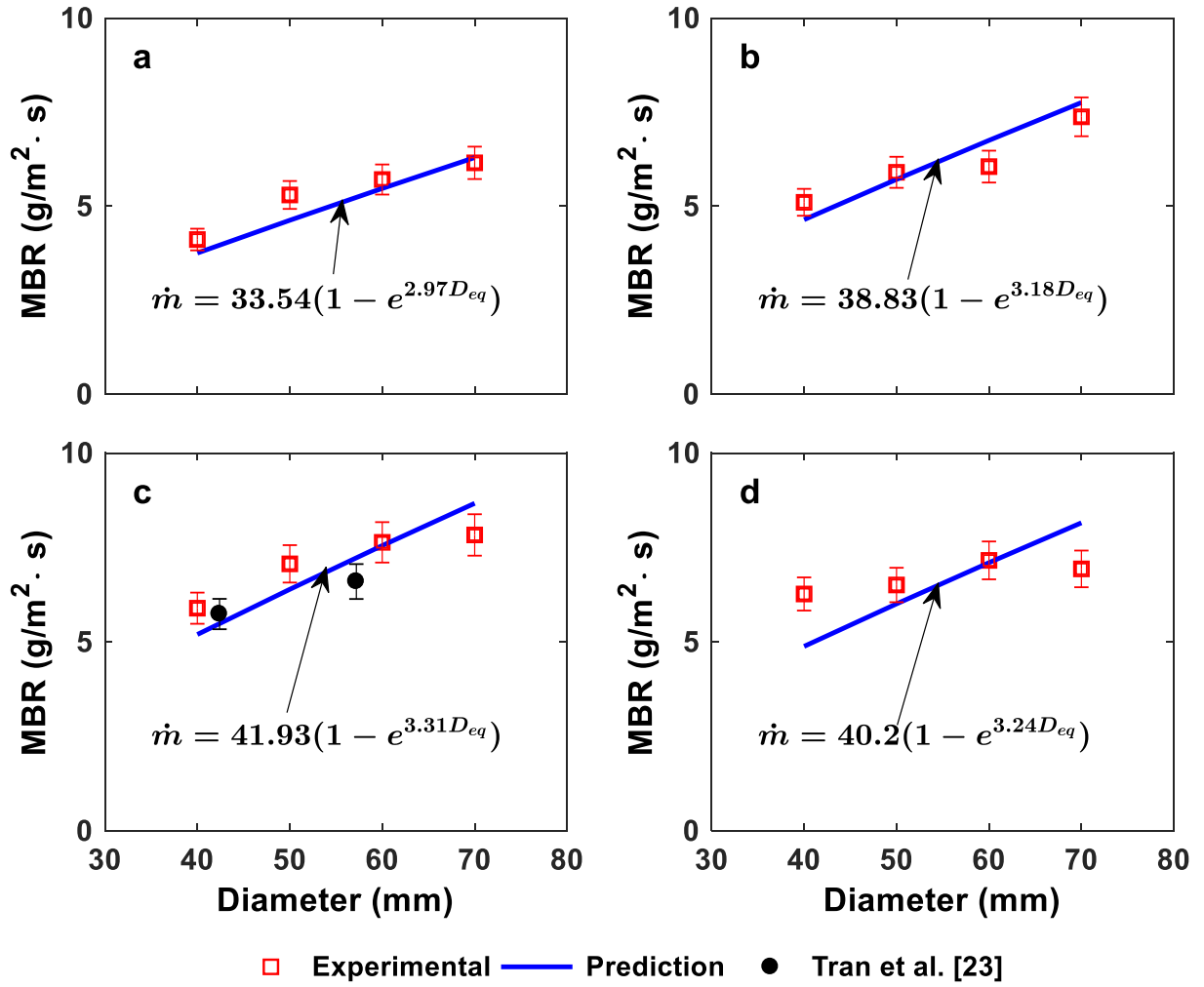


Fig. 5 The predicted MBR for (a) Diesel, (b) PME, (c) SME and (d) CME at different crucible size.

Despite Fig. 5 shows good correlation between experimental and predicted results, it should be emphasised that the proposed empirical correlation is applicable only to crucible diameter below 0.1 m, where the flow field of the flame is considerably laminar. The maximum MBR for diesel in Fig. 5 is lower than those reported by Chatris et al. [5] and Munoz et al. [35] by a factor of approximately two. This is presumably due to the prominence conductive heat transfer to the crucible wall that lowers the maximum achievable MBR in small crucible [20]. Since the variation in crucible diameter is only marginal in this study, it was assumed that variation of heat conduction rate to the crucible wall among crucibles are not significance. As such, heat conduction rate was assumed to be uniform for all crucibles examined. Moreover,

fuel height was kept at 20 mm for all types of fuels and crucibles examined, it was further assumed that the effect of lip height will be the same for all cases. Meanwhile, the constant  $k$  for the present study is higher than those reported by Chatris et al. [5] and Munoz et al. [35] by a factor of approximately 3-5. This is mainly due to  $k$  being more sensitive to the variation in crucible diameter in this regime (MBR is independent of the variation in crucible size when crucible is sufficiently large [36]).

### 3.2 Flame height

The pool fires appearance for diesel and neat biodiesels (PME, SME and CME) established with 40 and 60 mm crucibles are shown in Fig. 6. The flames established by all fuel types were bright, luminous orange-yellow, mainly due to the thermal radiation emitted by soot particles under pyrolytic condition. The heat generated from the flame decomposes the fuel molecules on the pool surface. These unoxidised fuel fragments subsequently collide and merge to form larger molecules, i.e. polycyclic aromatic hydrocarbon (PAH), which serves as the precursor for soot formation. The collision and condensation of PAHs form clusters that subsequently coagulate into soot particles [37].

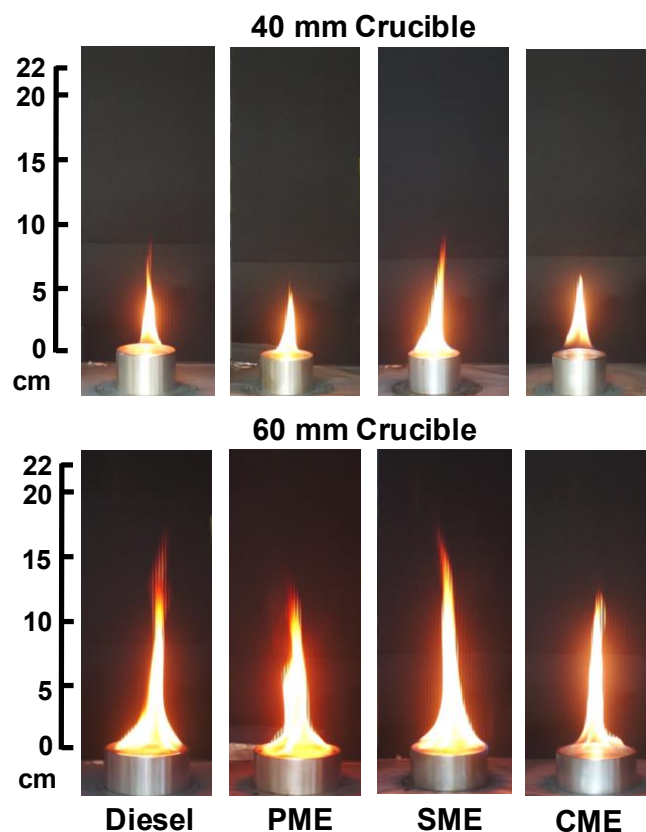


Fig. 6 Instantaneous flame images of diesel, PME, SME and CME established with 40 mm and 60 mm crucibles.

Figure 6 compares the flame height of diesel against neat biodiesels for 40 and 60 mm crucibles. Larger crucibles enable more fuel to be burned. Consequently, greater amount of air is entrained into the flame to react with the volatiles. The interaction between ambient air entrainment and lower density within the flame produces buoyancy-driven flows that inherently elevate the flame to a higher vertical position [20]. The Thomas correlation [38, 39] indicates that the non-dimensional flame height of a pool fire,  $L/D_{eq}$ , is a linear function of  $[\dot{m}/\rho_{\infty}\sqrt{gD_{eq}}]^{0.61}$ , where  $L$ ,  $\rho_{\infty}$ ,  $g$  represent the flame height, ambient air density and gravitational acceleration, respectively. Despite Thomas correlation was derived using highly turbulent flame (large pool fire), reviews by Heskestad [29] and Drysdale [20] had shown that gradients ( $m$ ) between normalised flame height and fuel burn rate parameter are not constant as fuel burn rate parameter varied. This signifies that different regimes have their own  $m$  and y-interception ( $c$ ). As such, the present study attempts to modify Thomas correlation for smaller crucibles with a considerably laminar flow field. The present research proposes that gradient ( $m$ ) and y-interception ( $c$ ) of Thomas correlation are correlated to  $\rho_f$  and cetane number  $CN$ , respectively, via empirical correlations as in Fig. 7. The Cetane number is a key parameter in internal combustion engines to assess the ignition properties of fuels. Since biodiesel is widely used as a replacement fuel for diesel fuel, cetane number is termed as a good parameter to correlate diesel and biodiesel with mass burning rate and flame height. The modified Thomas model is given by Eq. 2.

$$\frac{L}{D_{eq}} = (-5.15\rho_f + 5197) \left[ \frac{\dot{m}}{\rho_{\infty}\sqrt{gD_{eq}}} \right]^{0.61} + (-0.0175CN + 2.52) \quad (2)$$

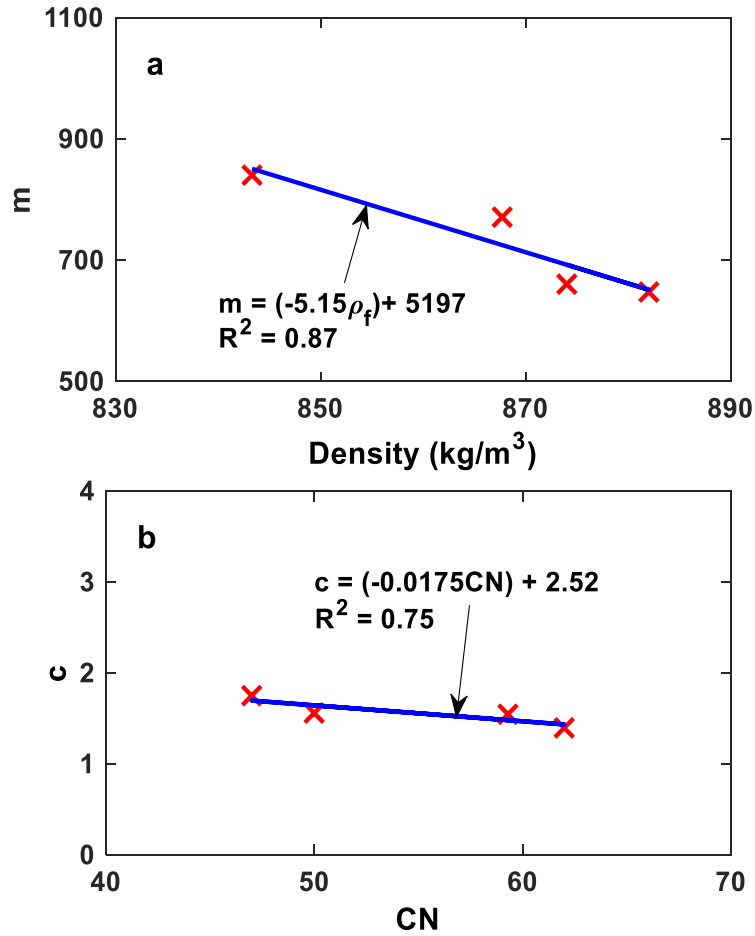


Fig. 7 Correlation of (a)  $m$  and (b)  $c$  as a function of fuel density and CN, respectively.

The experimental results published by Leite and Centeno [40] and Tran et al. [23] are included in Fig. 8a for validation purposes. It is demonstrated that Eq. 2 can estimate normalised diesel flame height from previous studies satisfactorily. Biodiesels flame heights estimated using Eq. 2 are plotted in Fig. 8b-d. Overall, the modified Thomas model shows good agreement with normalised diesel and biodiesels flame heights for  $6.71 \times 10^{-4} < [\dot{m}/\rho_\infty \sqrt{gD_{eq}}]^{0.61} < 1.87 \times 10^{-3}$ , indicating that Eq. 2 is capable of estimating flame height for biodiesel produced from a variety of feedstock for  $6.71 \times 10^{-4} < [\dot{m}/\rho_\infty \sqrt{gD_{eq}}]^{0.61} < 1.87 \times 10^{-3}$ , given that  $D_{eq}$ ,  $\rho_f$  and CN are known. The value for  $\dot{m}$  can be calculated via Eq. 1 and correlations from Fig. 4. This research unveils that existing empirical models for the relatively

large pool diameter can be modified for use in smaller pool diameter as well. The general trends also hint on the applicability of the model over various sizes.

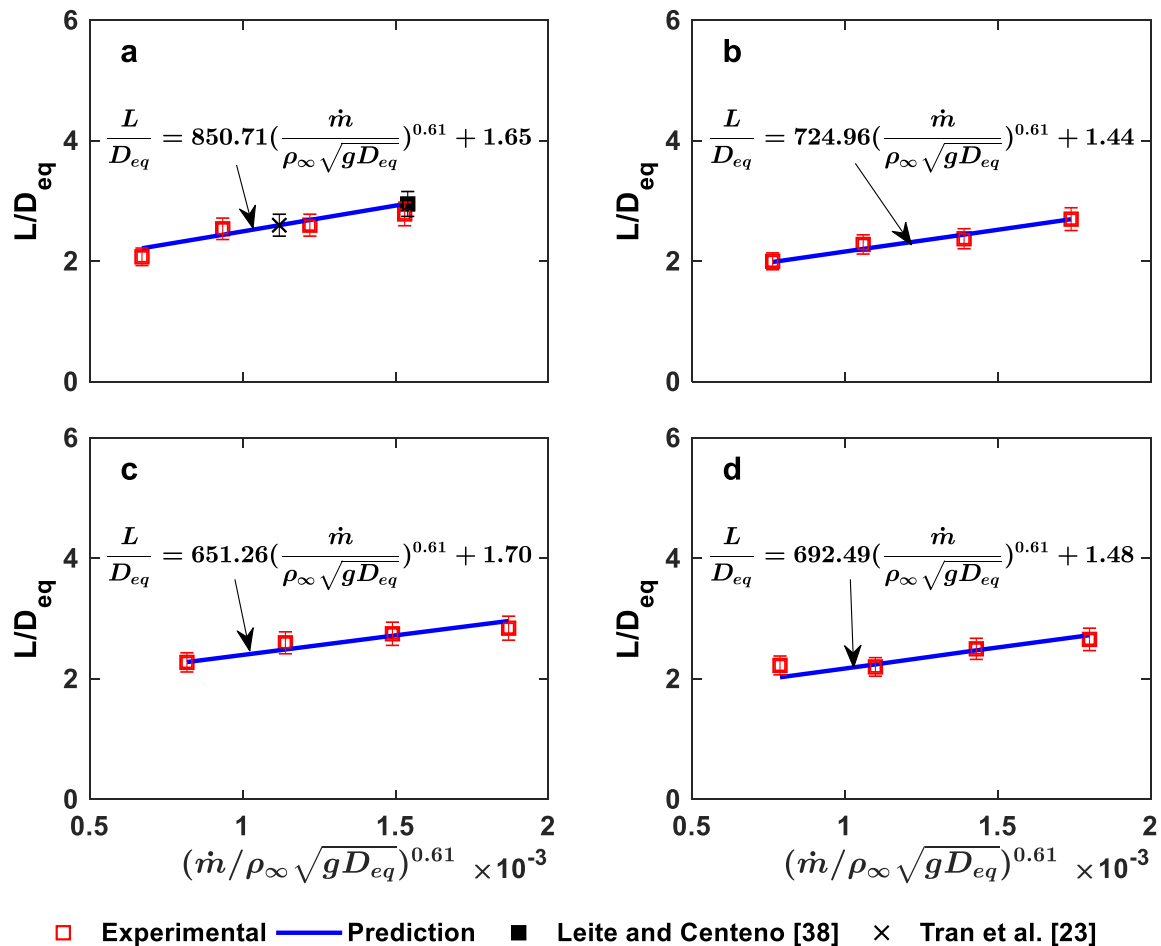


Fig. 8 (a) Diesel, (b) PME, (c) SME and (d) CME flame heights against respective mass burn parameter, based on Thomas correlation [38, 39].

Figure 8 also shows that flame height for diesel is marginally taller than biodiesels, despite the lower mass burning rate for the former (Fig. 3). This is primarily due to the higher sooting tendency for diesel. Soot particles that are not completely oxidised travel further downstream of the flame in search for oxidiser, thus extending the flame height [41]. Among the biodiesels tested, highly unsaturated SME tends to produce more soot than PME and CME [42], thus the flame height for SME is visibly taller than that of PME and CME.

### **3.3 Post-combustion Emissions**

#### **3.3.1 Carbon monoxide (CO)**

Production of CO is pronounced when the supply of oxygen is insufficient to oxidise all carbon into carbon dioxide. The CO emissions of different blends of SME, PME and CME are compared with diesel as shown in Fig. 9. The overall trend shows that specific CO emission reduces while increasing blend ratios for all crucible size. Neat biodiesels show the lowest CO emission level, with approximately a factor of 2-3 reduction as compared to B20. This indicates the effectiveness of biodiesel in suppressing CO emission under fuel-rich buoyancy-controlled diffusional burning modes. Although a general reduction trend of CO with respect to increasing biodiesel fraction is shown, some points such as those of PME B40 and PME B60 for 40 and 50 mm crucibles, respectively, show higher than expected values, probably due to the fact that buoyancy effects of the flame and the uneven vaporisation of the fuel from the pool surface are not quantified in the present setup. Figure 10 compares the CO emissions of neat biodiesels with diesel using different crucible sizes. The reduction of specific CO emissions for diesel is significant when increasing the crucible size, exhibiting an exponential decreasing trend. The flame height increases with crucible size. A taller flame is also subjected to greater amount of air entrainment, where more oxygen is introduced to convert CO into CO<sub>2</sub>. This explains the inverse trend of CO emission with the increase of crucible diameter.

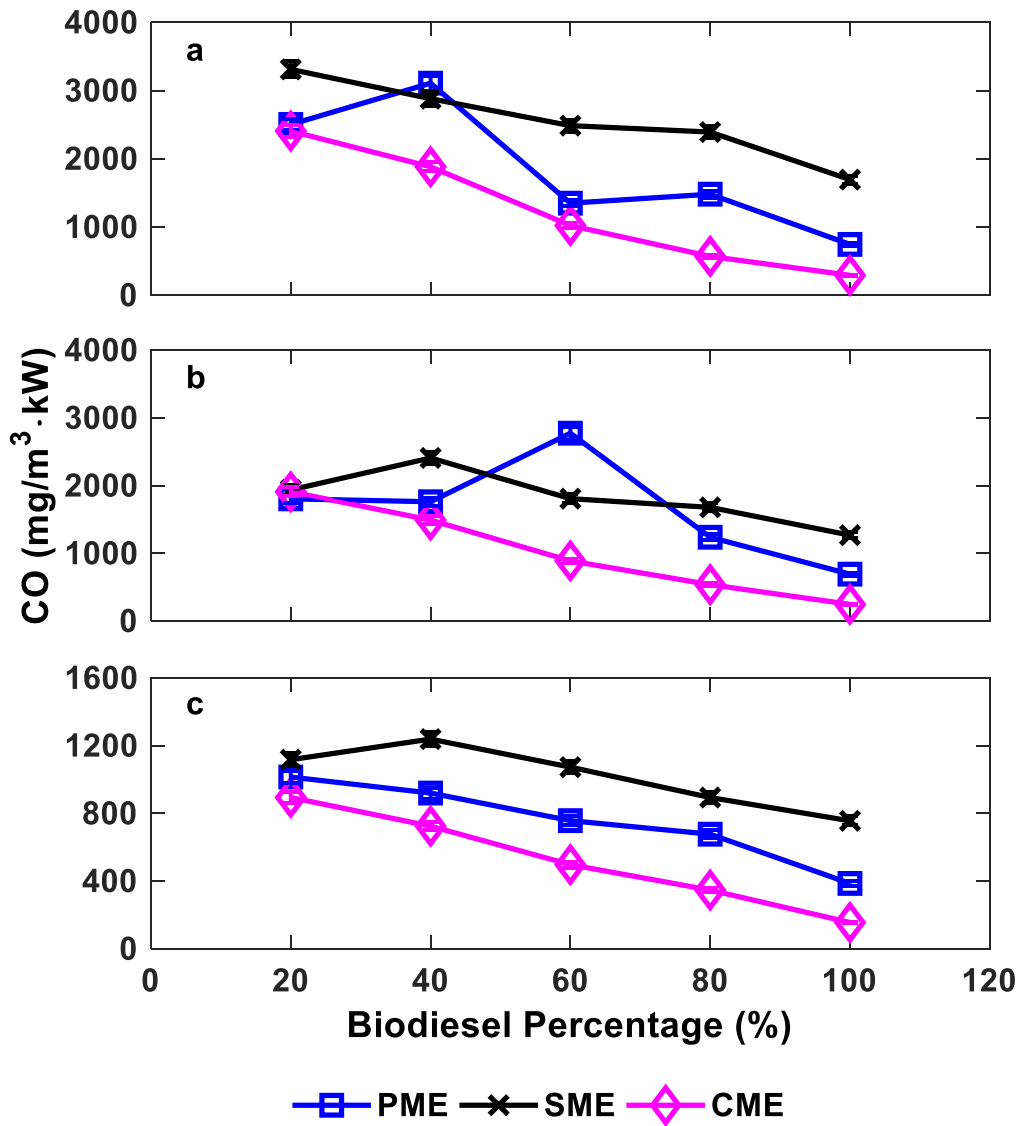


Fig. 9 Comparison of specific CO emission for different blend percentage of PME, SME and CME with diesel for (a) 40 (b) 50 and (c) 70 mm crucibles.



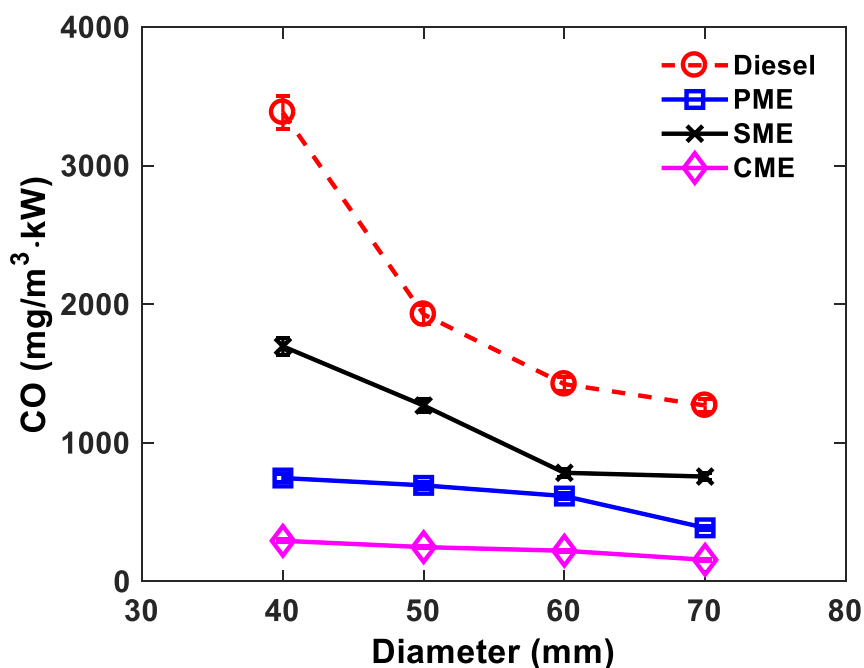


Fig. 10 Comparison of specific CO emission between PME, SME, CME and baseline diesel for different crucible sizes.

Biodiesel flames produce consistently lower CO compared to diesel for all used crucibles. As all the tests were conducted in the same quiescent environment, the lower CO emission for biodiesel as compared to diesel can be attributed to fuel-bonded oxygen, which serves as an additional oxygen supply to the combustion process that assists in the oxidation of CO into CO<sub>2</sub>. Among the tested biodiesels, results show that SME produces the highest CO, followed by PME and CME. This is because CME possesses the highest O/C ratio that enables further CO oxidation processes. SME contains the lowest O/C ratio, thus the CO emission level is the highest among all biodiesels. Meanwhile, the sooting tendency for biodiesel is another factor that may determine CO formation. SME produces higher soot levels as compared to PME and CME, mainly due to its highly unsaturated nature [25], leading to greater radiative heat loss that lowers the flame temperature and slows down CO oxidation rates [33, 43]. PME and CME that exhibit higher O/C ratios are expected to have higher flame temperature [33], thus facilitating CO oxidation, leading to lower CO emission [43].

### 3.3.2 Nitric oxide (NO)

Nitric oxide is produced by the oxidation of nitrogen during the combustion process. Comparison of the NO emissions of biodiesel blends with diesel for SME, PME and CME is shown in Fig. 11. In contrast to CO, NO emissions show an increasing trend with respect to the increase of biodiesel blend percentage. The increase of blend ratio from 20% to 80% resulted in the increase of NO by a factor of 2-3 for all blends. For the 70 mm crucible test, all three blend types exhibit similar NO levels, except at B100 when neat biodiesel was used. The increase of NO emission seems linear with the increase of blend percentage, especially for 50 and 70 mm crucibles.

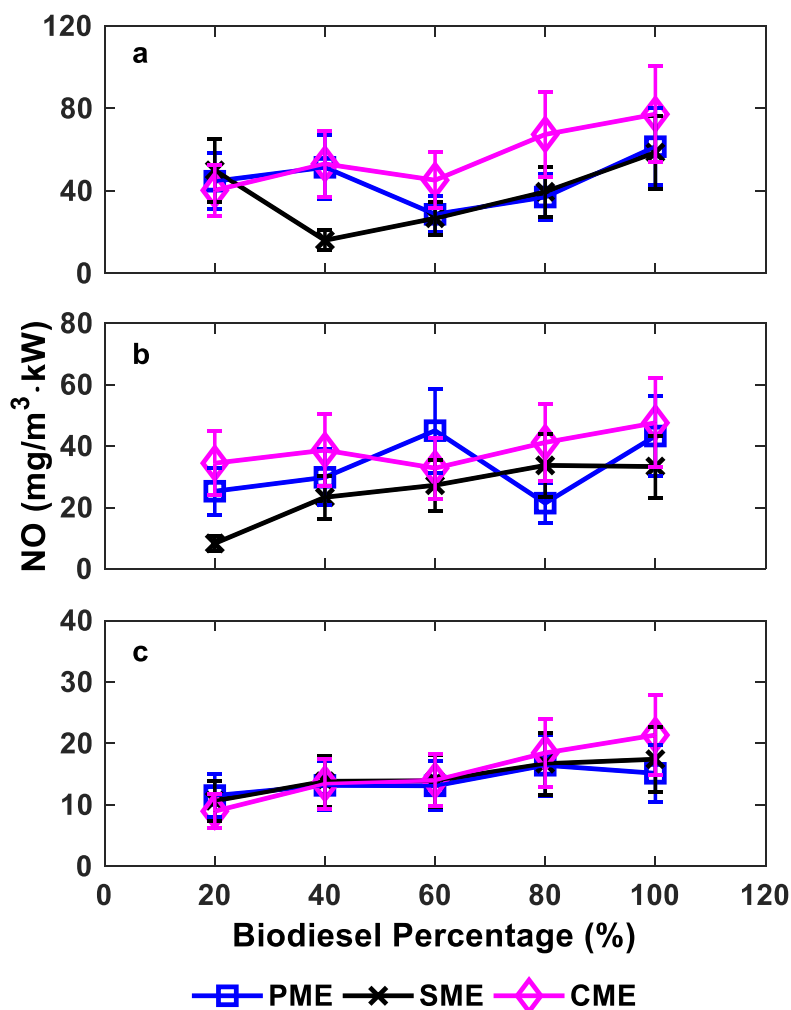


Fig. 11 Comparison of specific NO emission for different blend percentage of PME, SME and CME with diesel for (a) 40 (b) 50 and (c) 70 mm crucibles.

The NO emission of diesel and neat biodiesels are compared in Fig. 12 using different crucible sizes. It can be observed that both fuels show distinct NO reduction as the crucible inner diameter increases from 40 to 70 mm. This is partly due to higher amounts of air entrainment into the flame reaction area, resulting in overall flame temperature reduction. Another reason is the increased amount of oxygen available for complete oxidation into NO<sub>2</sub> (nitrogen dioxide) from NO.

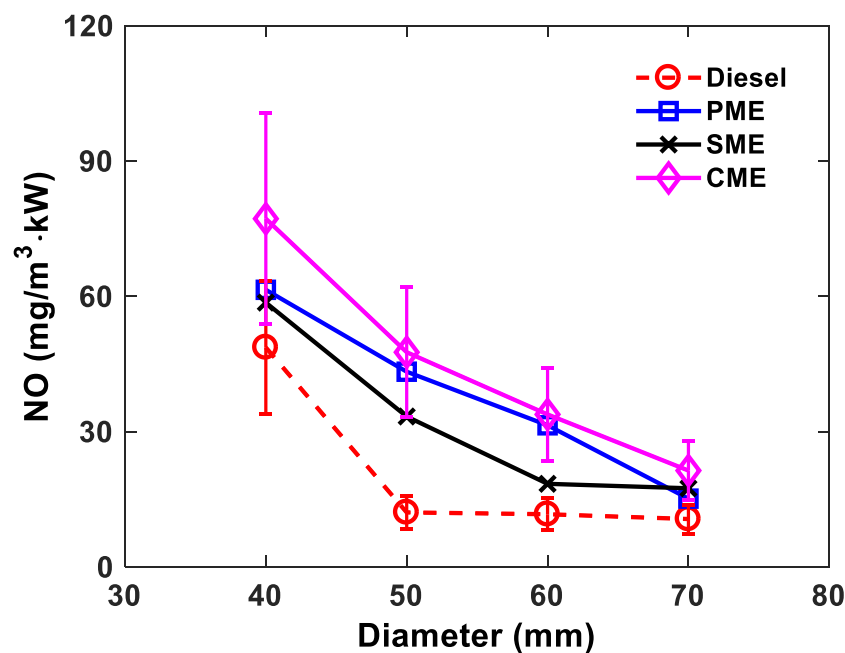


Fig. 12 Comparison of specific NO emission between PME, SME, CME and baseline diesel for different crucible sizes.

The higher emissions of NO for biodiesel can be attributed to the higher flame temperature which promotes NO production through thermal NO routes [33]. The NO produced via thermal mechanisms can be approximated by the equation  $[NO] = ke^{-K/T}[N_2][O_2]^{1/2}t$ , where  $T$  is the absolute temperature,  $t$  is residence time,  $k$  and  $K$  are reaction constant [44]. The biodiesel flame temperature is expected to be higher than for diesel, owing to the lower biodiesel sooting tendency that reduces radiative heat losses [33]. In

addition, the fuel-bond oxygen in the biodiesel molecule also assists in the local combustion and elevates the flame temperature, thus directly promoting thermal NO production. Comparison among the biodiesel shows that CME produces the highest NO levels, followed by PME and SME. The higher oxygen level in CME results in higher flame temperatures that contribute to higher thermal NO formation.

### **3.3.3 Sulphur Dioxide (SO<sub>2</sub>)**

Sulphur contained in the fuels will be converted into sulphur oxide (SO<sub>x</sub>) during combustion. Comparison of the specific SO<sub>2</sub> emissions as a function of biodiesel blends is shown in Fig. 13. The SO<sub>2</sub> emission level shows a general decreasing trend with increase of biodiesel percentage for all crucible sizes. This is expected as the sulphur content reduces with increasing the amount of biodiesel fraction in the fuel. Interestingly, a “surge” in value is seen for the case B60 for SME at 40 mm crucible size. The probable reason for the outlier could be the uneven liquid vaporisation caused by the buoyancy effect or the random error induced by the sensor in the gas analyser. For neat biodiesels, virtually no SO<sub>2</sub> was produced by the flame. Furthermore, the amount of SO<sub>2</sub> emission levels is comparable for all crucible sizes, which is within the range of 0-200 mg/m<sup>3</sup>.kW, although the 40 mm crucible tends to show slightly lower SO<sub>2</sub> on average due to lower mass burning rates. SME blends show higher tendency for SO<sub>2</sub> production, followed by PME and CME. The higher SO<sub>2</sub> emission by SME indicates that it contains higher sulphur contents than PME and CME.

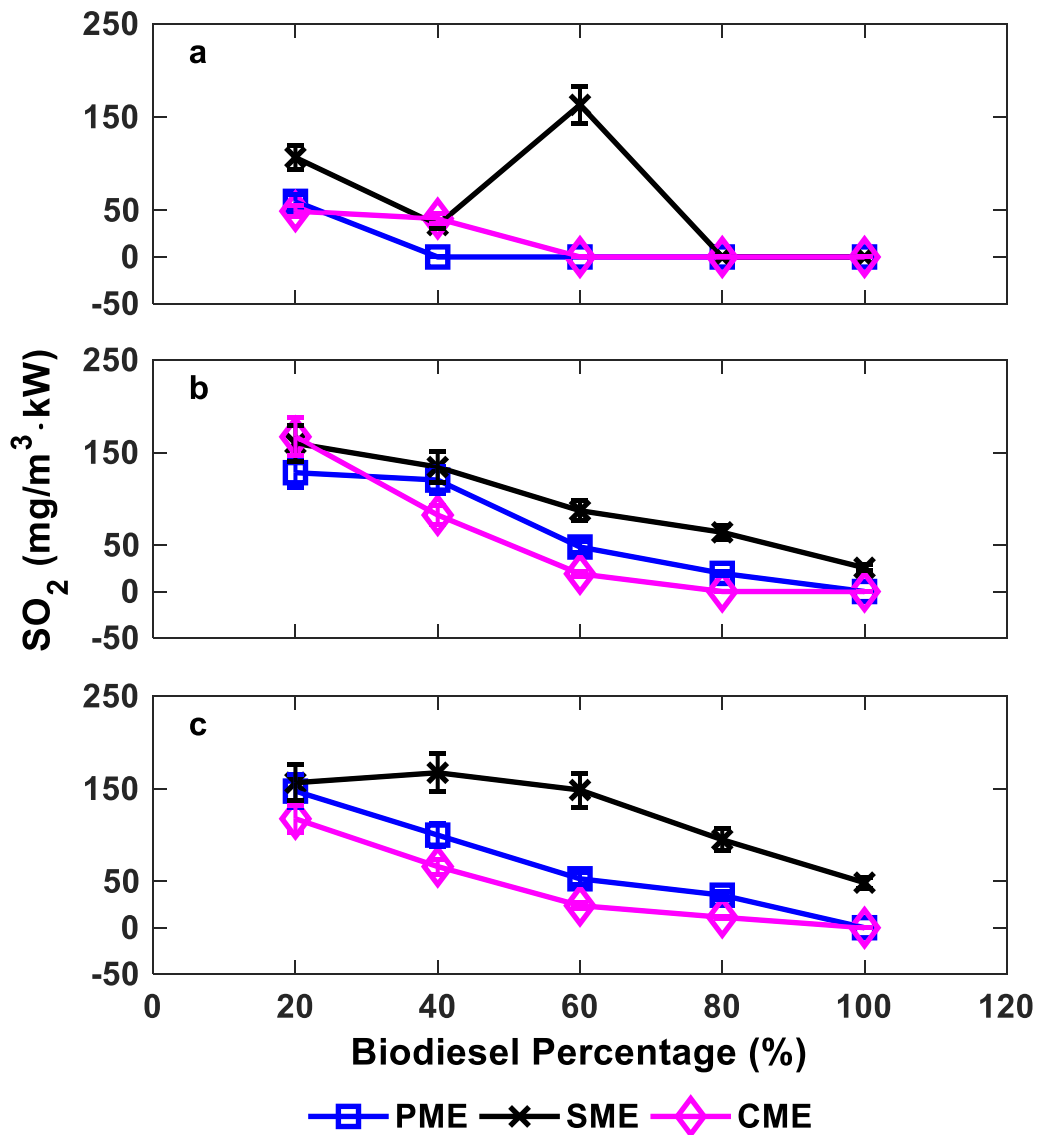


Fig. 13 Comparison of specific SO<sub>2</sub> emission for different blend percentage of PME, SME and CME with diesel for (a) 40 (b) 50 and (c) 70 mm crucibles.

Figure 14 compares the SO<sub>2</sub> emissions for diesel against that of neat biodiesels using different crucible sizes. Pure PME and CME produce virtually no SO<sub>2</sub>, while SME exhibits considerable increase of SO<sub>2</sub> emissions up to 50 mg/m<sup>3</sup>·kW as the crucible inner diameter increases from 40 to 70 mm. In contrast to biodiesels, diesel produces the highest level of SO<sub>2</sub> for all tested crucibles. The trace amount of sulphur in biodiesel is dwarfed when compared to fossil-based diesel. The reduced amount of SO<sub>2</sub> for biodiesel/diesel blends is desirable from

the perspective of regulating emissions, in particular for the transportation industry. In contrast to CO and NO, SO<sub>2</sub> emissions increase with the crucible size due to the increasing mass burning rate. The finding indicates that greater air entrainment for larger crucible does not dilute SO<sub>2</sub>.

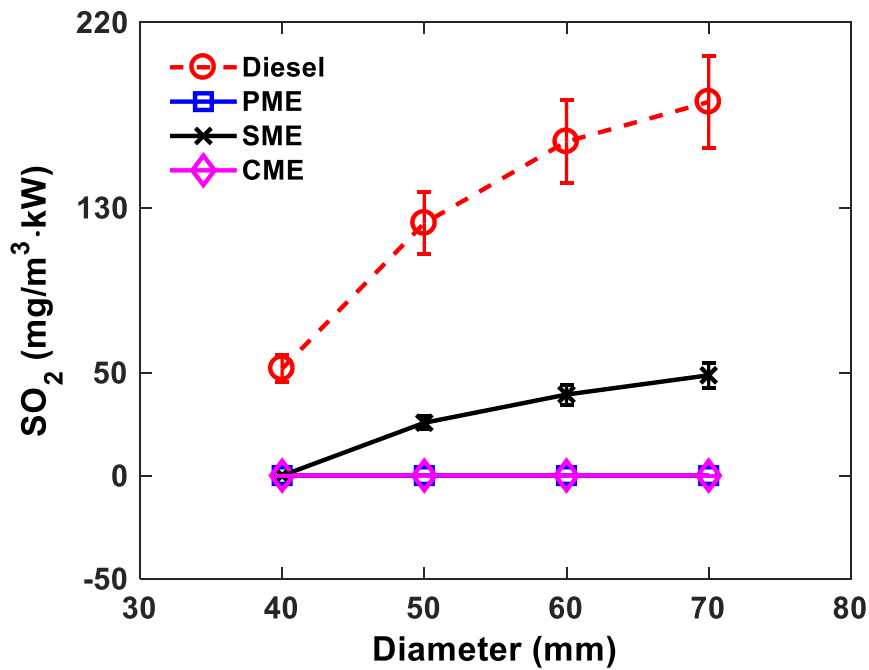


Fig. 14 Comparison of specific SO<sub>2</sub> emission between PME, SME, CME and baseline diesel for different crucible sizes.

#### 4.0 Conclusions

The burning characteristics of pool fires for diesel, SME, CME, PME and their blends with diesel were compared using crucibles of different diameters. The established pool fire shows distinct luminous orange-yellow profiles typical of diffusional flames, owing to the radiation from burning soot particles. Biodiesels exhibit higher mass burning rates compared to diesel, partly due to the oxygen content in the fuel that assists in the combustion process, higher density and lower radiative heat loss. Among the tested biodiesels, SME shows slightly higher mass burning rates than PME and CME. An empirical model for estimating fuel MBR was proposed in this study, which shows good agreement with experimental data. Thomas correlation was revised to estimate flame height. The revised model correlates well with experimental data for a range between  $6.71 \times 10^{-4} < [\dot{m} / \rho_{\infty} \sqrt{g D_{eq}}]^{0.61} < 1.87 \times 10^{-3}$ . The present study shows that existing empirical models for the relatively large pool fire can be modified for use in pool fires with smaller crucible sizes.

For the emission tests, biodiesels in general produced lower CO and higher NO as compared to diesel. The presence of oxygen in the biodiesel assists in more complete oxidation of CO into CO<sub>2</sub>, while concurrently assisting in localised combustion, elevating the flame temperature that leads to increase NO production. The effect of crucible size on specific CO and NO emissions is evident, as more air is entrained into the flame to assist oxidation, resulting in further reduction of specific CO and NO production. For SO<sub>2</sub> emissions, the sulphur is largely contributed by diesel, thus an increase in the biodiesel fraction in the blend results in reduced SO<sub>2</sub> emissions. SME shows slightly higher SO<sub>2</sub> as compared to PME and CME due to the inherent sulphur content in the fuel. The present study shows that the characteristics of pool fires are affected by the physio-chemical properties of the fuels, where biodiesel exhibits slightly different burning characteristics when compared to that of fossil diesel.

## References

1. Demirbas A (2007) Progress and recent trends in biofuels. *Prog Energy Combust Sci* 33:1–18
2. Shahir VK, Jawahar CP, Suresh PR (2015) Comparative study of diesel and biodiesel on CI engine with emphasis to emissions—A review. *Renew Sustain Energy Rev* 45:686–697
3. IEA (2017) *Technology Roadmap: Delivering Sustainable Bioenergy*
4. Koseki H, Mulholland GW (1991) The Effect of Diameter on the Burning of Crude Oil Pool Fires. *Fire Technol* 27:54–65
5. Chatris JM, Quintela J, Folch J, et al (2001) Experimental study of burning rate in jet-fuel pool fires. *Combust Flame* 126:1373–1383
6. Iwata Y, Koseki H, Janssens ML, Takahashi T (2001) Comparison of Combustion Characteristics of Various Crude Oils. *Int Assoc Fire Saf Sci* 7:1–7
7. Roh JS, Ryou HS, Kim DH, et al (2007) Critical velocity and burning rate in pool fire during longitudinal ventilation. *Tunn Undergr Sp Technol* 22:262–271
8. Roh JS, Yang SS, Ryou HS, et al (2008) An experimental study on the effect of ventilation velocity on burning rate in tunnel fires-heptane pool fire case. *Build Environ* 43:1225–1231
9. Woods JAR, Fleck BA, Kostiuk LW (2006) Effects of transverse air flow on burning rates of rectangular methanol pool fires. *Combust Flame* 146:379–390
10. Hu L, Liu S, Xu Y, Li D (2011) A wind tunnel experimental study on burning rate enhancement behavior of gasoline pool fires by cross air flow. *Combust Flame* 158:586–591
11. Hu L (2017) A review of physics and correlations of pool fire behaviour in wind and future challenges. *Fire Saf J* 91:41–55



12. Hu L, Liu S, Wu L (2013) Flame radiation feedback to fuel surface in medium ethanol and heptane pool fires with cross air flow. *Combust Flame* 160:295–306
13. Hu L, Hu J, Liu S, et al (2015) Evolution of heat feedback in medium pool fires with cross air flow and scaling of mass burning flux by a stagnant layer theory solution. *Proc Combust Inst* 35:2511–2518
14. Thomas PH, Webster CT, Raftery MM (1961) Some experiments on buoyant diffusion flames. *Combust Flame* 5:359–367
15. Heskestad G (1983) Luminous heights of turbulent diffusion flames. *Fire Saf J* 5:103–108
16. Yoshihara N, Ito A, Torikai H (2013) Flame characteristics of small-scale pool fires under low gravity environments. *Proc Combust Inst* 34:2599–2606
17. Abe H, Ito A, Torikai H (2015) Effect of gravity on puffing phenomenon of liquid pool fires. *Proc Combust Inst* 35:2581–2587
18. Tu R, Fang J, Zhang Y-M, et al (2013) Effects of low air pressure on radiation-controlled rectangular ethanol and n-heptane pool fires. *Proc Combust Inst* 34:2591–2598
19. Tang F, Hu L, Zhang X, et al (2015) Burning rate and flame tilt characteristics of radiation-controlled rectangular hydrocarbon pool fires with cross air flows in a reduced pressure. *Fuel* 139:18–25
20. Drysdale D (2011) *An Introduction to Flame Dynamics*. John Wiley and Sons
21. Smith DA, Cox G (1992) Major chemical species in buoyant turbulent diffusion flames. *Combust Flame* 91:226–238
22. Chen X, Lu S, Li C, et al (2014) Experimental study on ignition and combustion characteristics of typical oils. *Fire Mater* 38:409–417
23. Tran V, Morton C, Parthasarathy RN, Gollahalli SR (2014) Pool fires of biofuels and

- their blends with petroleum diesel. *Int J Green Energy* 11:595–610
24. Bazooyar B, Ebrahimzadeh E, Jomekian A, Shariati A (2014) NO<sub>x</sub> formation of biodiesel in utility power plant boilers. Part A: Influence of fuel characteristics. *Energy and Fuels* 28:3778–3792
  25. Tian B, Chong CT, Fan L, et al (2019) Soot volume fraction measurements over laminar pool flames of biofuels, diesel and blends. *Proc Combust Inst* 37:877–884
  26. Sun H, Wang C, Liu H, et al (2018) Burning Behavior and Parameter Analysis of Biodiesel Pool Fires. *Combust Sci Technol* 190:269–285
  27. Chiong MC, Chong CT, Ng J-H, et al (2018) Liquid biofuels production and emissions performance in gas turbines : A review. *Energy Convers Manag* 173:640–658
  28. Hoekman SK, Broch A, Robbins C, et al (2012) Review of biodiesel composition, properties, and specifications. *Renew Sustain Energy Rev* 16:143–169
  29. Heskestad G (2002) Fire Plumes, Flame Height, and Air Entrainment. In: *SFPE Handbook of Fire Protection Engineering*, 3rd ed
  30. Zukoski EE, Cetegen BM, Kubota T (1985) Visible structure of buoyant diffusion flames. *Symp Combust* 20:361–366
  31. Hamins A, Takashi K (1995) Characteristics of Pool Fire Burning. *Fire Resist. Ind. Fluids*
  32. Chiong MC, Chong CT, Ng J-H, et al (2018) Combustion and emission performances of coconut, palm and soybean methyl esters under reacting spray flame conditions. *J Energy Inst*
  33. Jha SK, Fernando S, To SDF (2008) Flame temperature analysis of biodiesel blends and components. *Fuel* 87:1982–1988
  34. Burgess D, Strasser A, Grumer J (1961) Diffusive burning of liquid fuels in open trays. *Symp Am Chem Soc* 91–106

35. Muñoz M, Arnaldos J, Casal J, Planas E (2004) Analysis of the geometric and radiative characteristics of hydrocarbon pool fires. *Combust Flame* 139:263–277
36. Babrauskas V (1983) Estimating large pool fire burning rates. *Fire Technol* 19:251–261
37. Gann R, Friedman R (2015) *Principles of Fire Behavior and Combustion*. Jones & Bartlett Learning
38. Thomas PH (1963) The size of flames from natural fires. *Symp Combust* 9:844–859
39. Sun H, Wang C, Liu H, et al (2017) Experimental Study of Combustion Characteristics of Circular Ring Thin-Layer Pool Fire. *Energy and Fuels* 31:10082–10092
40. Leite RM, Centeno FR (2018) Effect of tank diameter on thermal behavior of gasoline and diesel storage tanks fires. *J Hazard Mater* 342:544–552
41. Turns SR (2012) *An introduction to combustion: concepts and applications*, 3rd ed. McGrawHill
42. Kholghy MR, Weingarten J, Sediako AD, et al (2017) Structural effects of biodiesel on soot formation in a laminar coflow diffusion flame. *Proc Combust Inst* 36:1321–1328
43. Lefebvre AH, Ballal DR (2010) *Gas Turbine Combustion: Alternative Fuels and Emissions*, 3rd ed. CRC Press
44. Varatharajan K, Cheralathan M (2012) Influence of fuel properties and composition on NO<sub>x</sub> emissions from biodiesel powered diesel engines: A review. *Renew Sustain Energy Rev* 16:3702–3710